Direct Imaging of Antiferromagnetic Domains and Anomalous Layer-Dependent Mirror Symmetry Breaking in Atomically Thin $MnPS_3$

Zhuoliang Ni,[1] Huiqin Zhang,[2] David A. Hopper,[2,1] Amanda V. Haglund,[3] Nan Huang,[3] Deep Jariwala,[2] Lee C. Bassett,[2] David G. Mandrus,[3,4] Eugene J. Mele,[1] Charles L. Kane,[1] and Liang Wu[1,*]

[1]*Department of Physics and Astronomy, University of Pennsylvania, Philadelphia, Pennsylvania 19104, USA*
[2]*Department of Electrical and System Engineering, University of Pennsylvania, Philadelphia, Pennsylvania 19104, USA*
[3]*Department of Materials Science and Engineering, University of Tennessee, Knoxville, Tennessee 37996, USA*
[4]*Materials Science and Technology Division, Oak Ridge National Laboratory, Oak Ridge, Tennessee 37831, USA*

(Received 21 June 2021; revised 2 September 2021; accepted 5 October 2021; published 29 October 2021)

We have developed a sensitive cryogenic second-harmonic generation microscopy to study a van der Waals antiferromagnet $MnPS_3$. We find that long-range Néel antiferromagnetic order develops from the bulk crystal down to the bilayer, while it is absent in the monolayer. Before entering the long-range antiferromagnetic ordered phase in all samples, an upturn of the second harmonic generation below 200 K indicates the formation of the short-range order and magnetoelastic coupling. We also directly image the two antiphase (180°) antiferromagnetic domains and thermally induced domain switching down to bilayer. An anomalous mirror symmetry breaking shows up in samples thinner than ten layers for the temperature both above and below the Néel temperature, which indicates a structural change in few-layer samples. Minimal change of the second harmonic generation polar patterns in strain tuning experiments indicate that the symmetry crossover at ten layers is most likely an intrinsic property of $MnPS_3$ instead of an extrinsic origin of substrate-induced strain. Our results show that second harmonic generation microscopy is a direct tool for studying antiferromagnetic domains in atomically thin materials, and opens a new way to study two-dimensional antiferromagnets.

DOI: 10.1103/PhysRevLett.127.187201

Compared to ferromagnetic materials, antiferromagnetic (AFM) materials usually have a much higher magnon frequency in the terahertz regime and a more stable ground state to perturbations of external magnetic fields, making them promising platforms for spintronic devices operating in the terahertz frequency range. Two-dimensional (2D) AFM materials are of particular interest recently [1–15], with the prospect of devices down to the atomically thin limit. Contrary to the rapid development in 2D ferromagnetic materials [16–28], 2D AFM materials have been less explored due to the lack of direct probes on the AFM orders until very recently [9,12–14,29]. Raman scattering [1,2,4,5,30,31], magnetic tunneling [8], and magnon transport measurement reveal photons or the band gap coupled to the AFM orders [7], but they do not directly probe the AFM order and the domains [25].

Commonly known as a probe of structural and surface inversion symmetry ($\mathcal{P}$) breaking, second harmonic generation (SHG) has also been demonstrated to be a direct probe to the long-range AFM orders and domains [13,28,29,32,33]. SHG can be classified into two kinds: *i*-type and *c*-type [32,33]. The *i*-type SHG is invariant under the time-reversal symmetry ($\mathcal{T}$), and includes the electric-dipole (ED) SHG in noncentrosymmetric crystals and electric-quadruple (EQ) SHG. The EQ contribution does not require the condition of broken inversion symmetry in the lattice. The *c*-type SHG changes sign under the time-reversal transformation, and is only present if the spin structure breaks the inversion symmetry in centrosymmetric lattice. The *c*-type SHG has been very rare, and was observed in parity-time-reversal ($\mathcal{PT}$) symmetric antiferromagnets such as Cr_2O_3 [32,33], bilayer CrI_3 [28] and monolayer $MnPSe_3$ [13]. Below the transition temperature, the *c*-type SHG susceptibility is proportional to the order parameter [34]. The interference between the *c*-type and *i*-type SHG has been used to directly image AFM domains [13,32,33]. Nevertheless, studies on imaging of AFM domains in atomically thin crystals have been very limited [13,28].

The AFM transition metal thiophosphates MPS_3 (M = Mn, Fe, Ni) have attracted lots of interest recently including the many-body exciton in $NiPS_3$ [9,12,14], Ising antiferromagntism in $FePS_3$ [1,2,30,35], and the magnetoelectric effect in $MnPS_3$ [36]. Also, they order in different spin structures despite the same monoclinic structure in space group No. 12. $NiPS_3$ and $FePS_3$ have zigzag orders, but $MnPS_3$ has the Néel order. Among them, $MnPS_3$ breaks $\mathcal{P}$ and $\mathcal{T}$ below the Néel temperature (T_N), but respects $\mathcal{PT}$ symmetry, and, therefore, it allows the *c*-type ED SHG in the AFM phase. A previous SHG study on $MnPS_3$ demonstrated a phase-transition-like feature around T_N down to seven layer (7L), but did not observe short-range

order above T_N, Néel-type AFM domains, and did not provide a clear evidence for the c-type SHG that changes sign under time-reversal transformation [29]. Very high laser power was used in the previous study [29], because of the material's weak second-order response. Note that the SHG intensity from $MnPS_3$ is at least 2 orders of magnitude lower than that in $MnPSe_3$ due to its much weaker spin-orbital coupling [13]. Fast sample degradation due to high laser power happened within hours, which prevents a systematic study of the layer-dependent antiferromagnetism, domains, short-range order, and time-reversal-odd c-type SHG in $MnPS_3$ [29].

In this work, we develop a sensitive cryogenic scanning SHG microscopy with the photon detection sensitivity of 0.1 counts per second (c.p.s.) by using a photon counter to systematically study the layer-dependent antiferromagnetism in $MnPS_3$ down to the monolayer. We observe the sign change of the c-type SHG coefficient below T_N, and two antiphase (180°) AFM domains with spins reversed by time-reversal transformation. The long-range AFM order, evident from the c-type SHG, is present from the bulk to bilayer, but is absent in the monolayer. Between T_N and 200 K, we observe an increase of the SHG as a function of decreasing temperature, which indicates correlation-induced short-range order and the magnetoelastic coupling. Polarized SHG measurement shows the mirror-symmetry breaking below 10 L both below and above T_N, indicating a symmetry crossover in the structure in thin flakes.

The bulk crystal of $MnPS_3$ belongs to the point group of $2/m$ above $T_N \approx 78$ K and magnetic point group $2'/m$ below T_N. Neutron scattering measurements indicate its magnetic system to be Heisenberg type with tiny dipolar anisotropy and single-ion anisotropy [36–40]. The lattice structure is shown in Fig. 1(a). In the single layer, Mn atoms form a honeycomb lattice in the ab plane, and the two Mn atoms with opposite spin directions are marked by different colors, showing its AFM Néel order in a single layer. The spins are mainly out of plane, but 8° from the surface normal direction. The honeycomb layers stack along the c axis and with a shift of $1/3$ of the lattice constant along the a axis, which gives rise to a centrosymmetric lattice. There is a mirror symmetry perpendicular to the b axis. Interestingly, the formation of Néel AFM order breaks the inversion symmetry, and therefore it allows c-type ED SHG.

We first explore the SHG signal in a bulk crystal with thickness around 10 μm as shown in Fig. 1(d). Under normal incidence, we send in laser pulses centered at 800 nm (with 80 MHz repetition rate and around 50 fs duration) and measure SHG at 400 nm [13,41]. We focus 5 mW on a spot with a diameter of 10 μm. By consecutively doing thermal cycles at one spot, Fig. 1(b) shows that there are only two SHG traces when the crystal is cooled from the paramagnetic to the AFM states [42]. At high temperatures from 200 to 300 K, the temperature-independent SHG

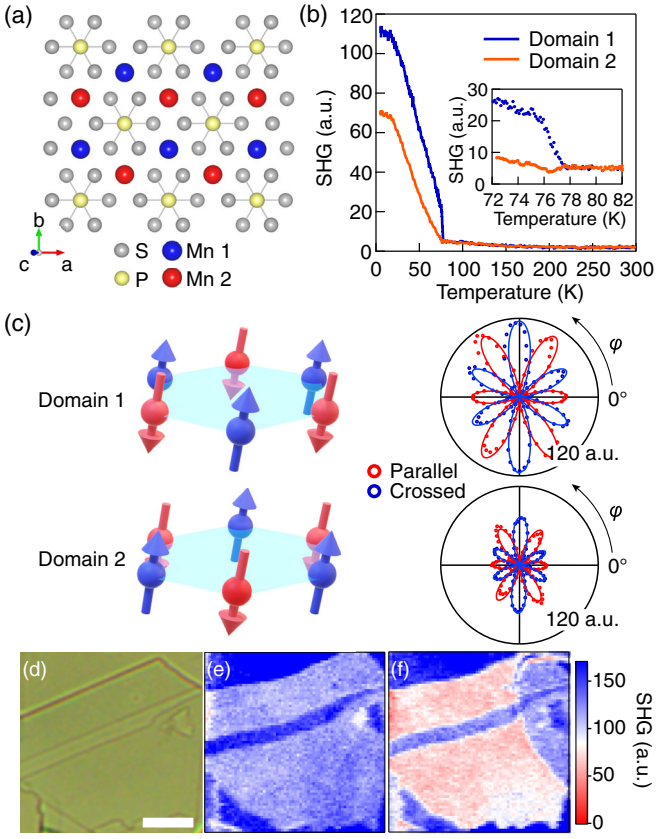

FIG. 1. (a) Top view of the monolayer crystal structure of $MnPS_3$. (b) Temperature dependence of SHG intensity of two domains in the same $MnPS_3$ bulk crystal. The inset shows SHG intensity near the transition temperature. (c) Two possible spin configurations of Mn atoms in a single layer. The arrows indicate spin directions of Mn atoms. The SHG polar patterns corresponding to two domains are shown on the right. The measured data are shown in dots and best fits are shown in solid lines. (d)–(f) Optical image and SHG intensity images at 5 K of a bulk $MnPS_3$ sample. Scale bar: 50 μm.

signal contributes from the electric-quadruple (EQ) term of the lattice. From 200 to 78 K (T_N), the two curves still overlap and rise gradually. The slow rising of the EQ term in SHG is believed to originate from short-range orders of spins due to correlation-induced lattice distortions [38], which is also known as magnetoelastic coupling [11]. A similar phenomenon was observed previously in a van der Waals ferromagnet [48]. The two curves split at 77.7(±0.3) K, which we define as the onset of c-type ED SHG and therefore the T_N. To explain the transition behavior, we write the interfering SHG intensity from ED and EQ terms as

$$I_i^{\mathrm{SHG}} = [\pm\chi_{ijk}^{\mathrm{ED}}(T \le T_N)E_jE_k + \chi_{ijkl}^{\mathrm{EQ}}(T)E_j\nabla_k E_l]^2, \quad (1)$$

where $\chi_{ijk}^{\mathrm{ED}}(T) \propto M \propto (T_N - T)^{\beta}$ is the ED SHG coefficient [34]. (M is the staggered magnetization of the two Mn sites and is the order parameter.) The ± sign corresponding to

two $\mathcal{PT}$-related domains as shown in Fig. 1(c). $\chi^{\mathrm{EQ}}(T)$ is present at all temperatures and is identical in both domains, since magnetoelastic distortions caused by the two domains are the same. The splitting of SHG intensity of the two domains at T_N is the direct evidence of the time-reversal-odd c-type ED SHG and therefore the long-range AFM order in $MnPS_3$. As observed in a centrosymmetric 2D ferromagnet [48] and the 2D zigzag antiferromagnet $NiPS_3$ [42], just observing the rising of SHG across T_N without observing a sign change could contribute from i-type SHG due to magnetoelastic coupling and might not be proportional to the order parameter. Note that the inset figure in Fig. 1(b) shows a change of slope in the curve of domain 1 around 76 K, which might be related with the crossover of 3D to 2D critical behavior [38,42].

Figures 1(e) and 1(f) show SHG intensity mapping at 5 K after two consecutive thermal cycles in the area marked by the optical image in Fig. 1(d). Figure 1(e) shows a single domain, while Fig. 1(f) shows two domains. To the best of our knowledge, this is the first report of direct observation of AFM domains in $MnPS_3$. We further measure the SHG polar patterns in these two domains as shown on the right of Fig. 1(b). Here "parallel" and "crossed" refer to configurations of the polarization of the incident and SHG laser pulses [13,41], and they have different angle dependence on χ^{ED}_{ijk}, which reveal the symmetry of the material (see Supplemental Material S1 [42]). The $\phi = 0$ direction in parallel configuration corresponds to the a axis of the $MnPS_3$ crystal. These patterns can be well fitted (solid lines) by the symmetry analysis based on the material's space group. The SHG maps in Figs. 1(e), 1(f) and traces in Fig. 1(b) are taken when $\phi = 0°$ in the parallel configuration. We fix the laser position at one spot, and confirm that there are only two kinds of polar patterns after ten thermal cycles. The two domains switch to each other by the time-reversal transformation. As a result, the c-type ED SHG is also called nonreciprocal SHG. The polar patterns also confirm that the mirror plane perpendicular to the b axis and the tilting angle of spins are in the ac plane.

Next, we study whether the long-range order and domains sustain in the atomically thin limit. We use a relatively low power of 2 mW over the beam diameter of 10 μm to avoid damage to atomically thin samples. Note that our incident power per area is around 50 times lower than that of the previous study [29]. The optical image of a large nine-layer (9L) sample on SiO_2(90 nm)/Si(0.5 mm) is shown Fig. 2(a), and the thickness is determined by a combination of atomic force microscopy measurement and color contrast measurement [42]. We perform a SHG mapping at 5 K [Fig. 2(b)] with the polarization at 172° peak position in the parallel configuration of domain 1 in Fig. 2(e). Two AFM domains are observed represented by the darker (domain 2) and the brighter (domain 1) areas. Next, we warm up the sample above T_N and cool it back to 5 K, and the new SHG mapping is shown as Fig. 2(c).

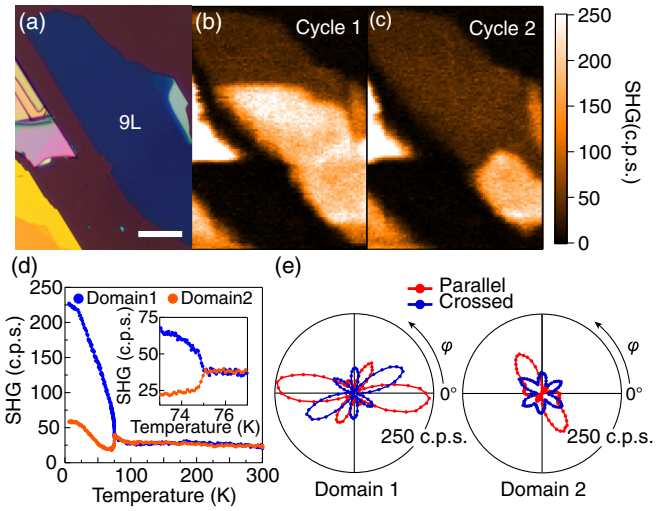

FIG. 2. (a) Optical image of the 9 L $MnPS_3$ sample. Scale bar: 20 μm. (b)–(c) SHG intensity mapping measured at 5 K. (d) Temperature dependence of SHG intensity of two domains Inset shows a closer look near transition temperature. (e) Polarization dependence of SHG intensity of two domains measured at 5 K.

The different distribution of two domains indicates that Néel vectors switch freely between two directions across T_N, in consistency with the bulk. Figure 2(d) shows the temperature-dependent intensity of two domains with $\phi = 172°$ in the parallel configuration. We also perform over nine thermal cycles and confirm that there are only two domains [42]. Surprisingly, both polar patterns in Fig. 2(e) show the breaking of mirror symmetry in the spin structure of this 9L sample.

To approach the 2D limit, we exfoliate $MnPS_3$ samples from six layer to monolayer. The isolated samples with diameters at least 3 times larger than the laser spot are chosen. The experimental results are summarized in Fig. 3. Polar patterns of the two domains at 5 K in 2,3,5,6-layer samples are shown in Fig. 3(a). Similar to the 9L sample, the mirror symmetry is broken in these samples. The temperature-dependent SHG intensity of these samples is shown in Fig. 3(b). The layer-dependent intensity at 5 K (chosen at the maximum in the parallel pattern) is shown in Fig. 3(c). As each $MnPS_3$ layer produces in-phase SHG response, the intensity of samples from 3 to 22 L nearly follows the dependence of the square of the number of layers, as observed in other inversion-breaking 2D materials [13,49]. There is a strong suppression of SHG intensity in the bilayer samples. We confirm that the suppression is not due to degradation in air as the SHG intensity of a 2 L sample exfoliated in a glove box is the same [42]. We measure three monolayer samples exfoliated in air and one monolayer sample exfoliated in the glove box, but we are unable to detect a temperature-dependent SHG signal within our setup sensitivity of 0.1 c.p.s. [42]. Therefore, we think the absence of long-range order in the monolayer is not due to air degradation. The Néel temperature, which

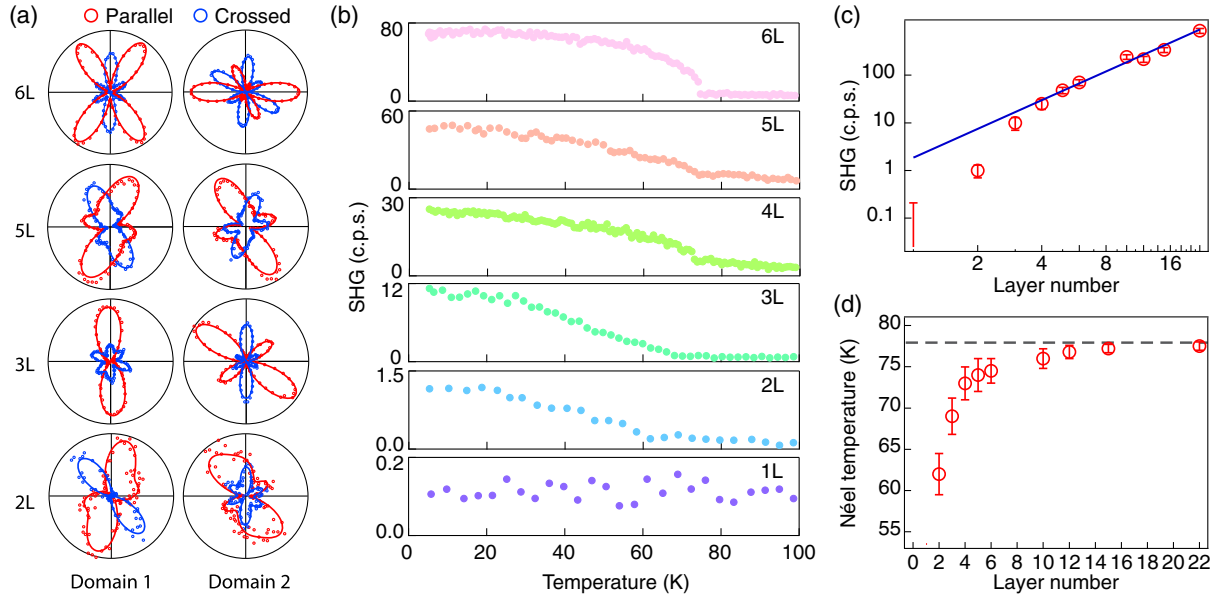

FIG. 3. (a) SHG polar patterns of two AFM domains in different layers measured at 5 K. (b) Temperature dependence of SHG intensity at the crossed peak of domain 1 from different layers. (c) Layer number dependence of SHG intensity. (d) Layer number dependence of Néel temperature.

we extract at the splitting of SHG of two domains, is plotted in Fig. 3(d). It is also suppressed with decreasing of the layer number (below 10 L).

In order to study the origin of the mirror symmetry breaking, we systematically investigate the layer dependence. As shown in Fig. 4, there is a clear difference between the 12 and the 10 L samples. For samples thicker than 12 L, the SHG patterns show a mirror symmetry, and the six lobes are of comparable magnitude, which is similar to the bulk sample in Fig. 1. However, for those thinner than 10 L, the mirror symmetry is absent in 10 K, similar to the data shown in Figs. 2 and 3. Note that at 200 K, where the EQ SHG signal is mostly from the lattice and is decoupled to the short-range spin correlation, the mirror symmetry is still absent. Therefore, the absence of the mirror symmetry below 10 L has a lattice origin. A recently near-field infrared spectroscopy study on the phonon spectrum and density functional theory calculation on the same material also shows a crossover of the lattice symmetry around 10 L, and they attribute it to the symmetry crossover from $2/m$ to a higher symmetry $P3_1m$ with three mirrors [50,51]. In our experiment, though observing the similar thickness for the crossover, we find the symmetry of $MnPS_3$ samples thinner than 10 L in the paramagnetic state is actually lower than thicker samples. We tend to believe that the mirror symmetry breaking is an intrinsic property of very thin $MnPS_3$ crystal as the change of polar patterns between 12 and 10 L is dramatic. We tend to think that mirror symmetry breaking is not due to stacking faults as it has a systematic thickness dependence. Also, to exclude the strain effect caused by the substrate, we perform the strain-tuning experiments on 9 and a 16 L samples. No strain-induced mirror symmetry breaking is observed in the 16 L sample. Also, both samples do not show the change in the SHG polar pattern by the 5% strain applied on the substrate [42].

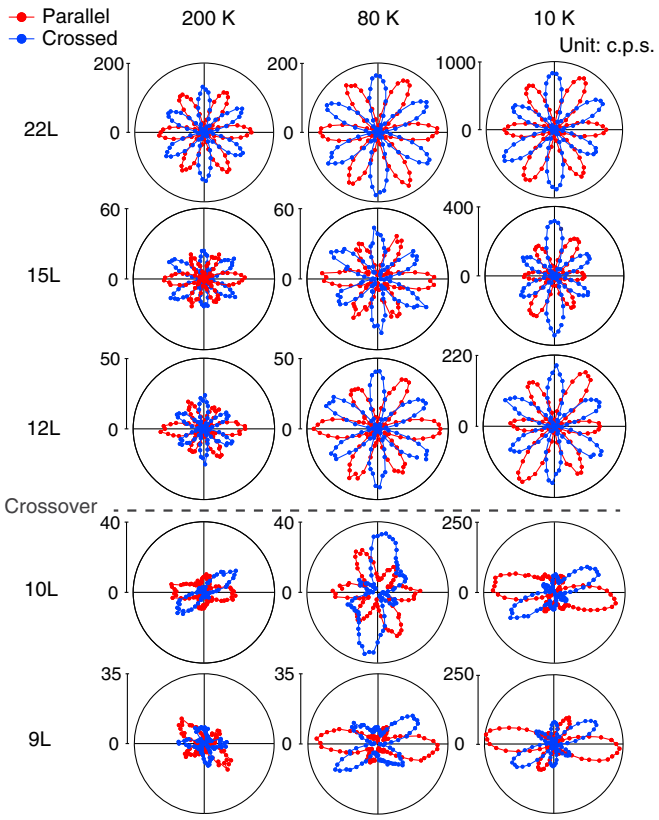

FIG. 4. Parallel (red) and crossed (blue) polar patterns of different layers. The dots with lines are the data.

Further detailed structure measurement and density functional theory calculations are called to reveal the origin of mirror symmetry breaking below 10 L.

The long-range order in bulk $MnPS_3$ is believed to result from the anisotropy and the weak interplanar coupling [37,38]. The suppression of the Néel temperature possibly results from reduced interplanar coupling in atomically thin samples [6,17]. Nevertheless, considering the symmetry of the spin structure is different in samples less than 10 L, it might not be valid to use the same bulk Hamiltonian to explain atomically thin samples. We also cannot rule out the possibility of disorder effect on the absence of the ordering in the monolayer. More discussions about the suppression of long-range order in the monolayer can be found in Ref. [42]. We hope more future works will investigate the monolayer $MnPS_3$.

To summarize, by using a sensitive SHG microscopy, we systematically study the layer dependence of AFM states in $MnPS_3$, and observe the switching of Néel-type AFM domains. Looking forward, We believe that this work is critical to understanding the 2D antiferromagnetism in this compound, and application for 2D terahertz AFM spintronic devices.

We thank S. W. Cheong for helpful discussions. The project design, data collection, and analysis are supported by L. W.'s startup package at the University of Pennsylvania. The development of the SHG photon counter is supported by the ARO YIP Award under the Grant No. W911NF1910342. The development of the scanning SHG imaging microscope is partially supported by the ARO DURIP Award under the Grant No. W911NF2110131. The measurement by the atomic force microscopy is supported by the ARO MURI under the Grant No. W911NF2020166. Z. N., H. Z., D. A. H., D. J., L. C. B., and L. W. acknowledge partial support from the National Science Foundation supported University of Pennsylvania Materials Research Science and Engineering Center (MRSEC) (DMR-1720530). E. J. M. acknowledges support from NSF EAGER 1838456. C. L. K. is supported by a Simons Investigator grant from the Simons Foundation. D. G. M. acknowledges support from the Gordon and Betty Moore Foundation's EPiQS Initiative, Grant No. GBMF9069. This work was carried out in part at the Singh Center for Nanotechnology, which is supported by the NSF National Nanotechnology Coordinated Infrastructure Program under Grant No. NNCI-1542153. Z. N. and H. Z. also acknowledge support from the Vagelos Institute of Energy Science and Technology graduate fellowship at the University of Pennsylvania.

*liangwu@sas.upenn.edu

[1] J.-U. Lee, S. Lee, J. H. Ryoo, S. Kang, T. Yun Kim, P. Kim, C.-H. Park, J.-G. Park, and H. Cheong, Ising-type magnetic ordering in atomically thin $FePS_3$, Nano Lett. **16**, 7433 (2016).

[2] X. Wang, K. Du, Y. Y. F. Liu, P. Hu, J. Zhang, Q. Zhang, M. H. S. Owen, X. Lu, C. K. Gan, and P. Sengupta, Raman spectroscopy of atomically thin two-dimensional magnetic iron phosphorus trisulfide ($FePS_3$) crystals, 2D Mater. **3**, 031009 (2016).

[3] S. Y. Kim, T. Y. Kim, L. J. Sandilands, S. Sinn, M.-C. Lee, J. Son, S. Lee, K.-Y. Choi, W. Kim, B.-G. Park, C. Jeon, H.-D. Kim, C.-H. Park, J.-G. Park, S. J. Moon, and T. W. Noh, Charge-Spin Correlation in van der Waals Antiferromagnet $NiPS_3$, Phys. Rev. Lett. **120**, 136402 (2018).

[4] Y.-J. Sun, Q.-H. Tan, X.-L. Liu, Y.-F. Gao, and J. Zhang, Probing the magnetic ordering of antiferromagnetic $MnPS_3$ by Raman spectroscopy, J. Phys. Chem. **10**, 3087 (2019).

[5] K. Kim, S. Y. Lim, J. Kim, J.-U. Lee, S. Lee, P. Kim, K. Park, S. Son, C.-H. Park, J.-G. Park, and H. Cheong, Antiferromagnetic ordering in van der Waals 2D magnetic material $MnPS_3$ probed by Raman spectroscopy, 2D Mater. **6**, 041001 (2019).

[6] K. Kim, S. Y. Lim, J.-U. Lee, S. Lee, T. Yun Kim, K. Park, G. S. Jeon, C.-H. Park, J.-G. Park, and H. Cheong, Suppression of magnetic ordering in XXZ-type antiferromagnetic monolayer $NiPS_3$, Nat. Commun. **10**, 345 (2019).

[7] W. Xing, L. Qiu, X. Wang, Y. Yao, Y. Ma, R. Cai, S. Jia, X. C. Xie, and W. Han, Magnon Transport in Quasi-Two-Dimensional van der Waals Antiferromagnets, Phys. Rev. X **9**, 011026 (2019).

[8] G. Long, H. Henck, M. Gibertini, D. Dumcenco, Z. Wang, T. Taniguchi, K. Watanabe, E. Giannini, and A. F. Morpurgo, Persistence of magnetism in atomically thin $MnPS_3$ crystals, Nano Lett. **20**, 2452 (2020).

[9] S. Kang *et al.*, Coherent many-body exciton in van der Waals antiferromagnet $NiPS_3$, Nature (London) **583**, 785 (2020).

[10] M. Šiškins, M. Lee, S. Mañas-Valero, E. Coronado, Y. M. Blanter, H. S. J. van der Zant, and P. G. Steeneken, Magnetic and electronic phase transitions probed by nanomechanical resonators, Nat. Commun. **11**, 2698 (2020).

[11] D. Vaclavkova, A. Delhomme, C. Faugeras, M. Potemski, A. Bogucki, J. Suffczyński, P. Kossacki, A. R. Wildes, B. Grémaud, and A. Saúl, Magnetoelastic interaction in the two-dimensional magnetic material $MnPS_3$ studied by first principles calculations and Raman experiments, 2D Mater. **7**, 035030 (2020).

[12] X. Wang, J. Cao, Z. Lu, A. Cohen, H. Kitadai, T. Li, Q. Tan, M. Wilson, C. H. Lui, D. Smirnov *et al.*, Spin-induced linear polarization of photoluminescence in antiferromagnetic van der Waals crystals, Nat. Mater. **20**, 964 (2021).

[13] Z. Ni, A. V. Haglund, H. Wang, B. Xu, C. Bernhard, D. G. Mandrus, X. Qian, E. J. Mele, C. L. Kane, and L. Wu, Imaging the Néel vector switching in the monolayer antiferromagnet $MnPSe_3$ with strain-controlled Ising order, Nat. Nanotechnol. **16**, 782 (2021).

[14] K. Hwangbo, Q. Zhang, Q. Jiang, Y. Wang, J. Fonseca, C. Wang, G. M. Diederich, D. R. Gamelin, D. Xiao, J.-H. Chu, W. Yao, and X. Xu, Highly anisotropic excitons and multiple phonon bound states in a van der Waals antiferromagnetic insulator, Nat. Nanotechnol. **16**, 655 (2021).

[15] D. Afanasiev, J. R. Hortensius, M. Matthiesen, S. Mañas-Valero, M. Šiškins, M. Lee, E. Lesne, H. S. J. van der Zant, P. G. Steeneken, B. A. Ivanov, E. Coronado, and

A. D. Caviglia, Controlling the anisotropy of a van der waals antiferromagnet with light, Sci. Adv. **7**, eabf3096 (2021).

[16] B. Huang, G. Clark, E. Navarro-Moratalla, D. R. Klein, R. Cheng, K. L. Seyler, D. Zhong, E. Schmidgall, M. A. McGuire, D. H. Cobden, W. Yao, D. Xiao, P. Jarillo-Herrero, and X. Xu, Layer-dependent ferromagnetism in a van der Waals crystal down to the monolayer limit, Nature (London) **546**, 270 (2017).

[17] C. Gong, L. Li, Z. Li, H. Ji, A. Stern, Y. Xia, T. Cao, W. Bao, C. Wang, and Y. Wang, Discovery of intrinsic ferromagnetism in two-dimensional van der Waals crystals, Nature (London) **546**, 265 (2017).

[18] W. Chen, Z. Sun, Z. Wang, L. Gu, X. Xu, S. Wu, and C. Gao, Direct observation of van der Waals stacking dependent interlayer magnetism, Science **366**, 983 (2019).

[19] L. Thiel, Z. Wang, M. A. Tschudin, D. Rohner, I. Gutiérrez-Lezama, N. Ubrig, M. Gibertini, E. Giannini, A. F. Morpurgo, and P. Maletinsky, Probing magnetism in 2D materials at the nanoscale with single-spin microscopy, Science **364**, 973 (2019).

[20] D. R. Klein, D. MacNeill, J. L. Lado, D. Soriano, E. Navarro-Moratalla, K. Watanabe, T. Taniguchi, S. Manni, P. Canfield, and J. Fernández-Rossier, Probing magnetism in 2D van der Waals crystalline insulators via electron tunneling, Science **360**, 1218 (2018).

[21] T. Song, X. Cai, M. W.-Y. Tu, X. Zhang, B. Huang, N. P. Wilson, K. L. Seyler, L. Zhu, T. Taniguchi, and K. Watanabe, Giant tunneling magnetoresistance in spin-filter van der Waals heterostructures, Science **360**, 1214 (2018).

[22] K. S. Burch, D. Mandrus, and J.-G. Park, Magnetism in two-dimensional van der Waals materials, Nature (London) **563**, 47 (2018).

[23] B. Huang, G. Clark, D. R. Klein, D. MacNeill, E. Navarro-Moratalla, K. L. Seyler, N. Wilson, M. A. McGuire, D. H. Cobden, D. Xiao *et al.*, Electrical control of 2D magnetism in bilayer CrI_3, Nat. Nanotechnol. **13**, 544 (2018).

[24] Y. Deng, Y. Yu, Y. Song, J. Zhang, N. Z. Wang, Z. Sun, Y. Yi, Y. Z. Wu, S. Wu, J. Zhu, J. Wang, X. H. Chen, and Y. Zhang, Gate-tunable room-temperature ferromagnetism in two-dimensional Fe_3GeTe_2, Nature (London) **563**, 94 (2018).

[25] K. F. Mak, J. Shan, and D. C. Ralph, Probing and controlling magnetic states in 2D layered magnetic materials, Nat. Rev. Phys. **1**, 646 (2019).

[26] C. Gong and X. Zhang, Two-dimensional magnetic crystals and emergent heterostructure devices, Science **363**, eaav4450 (2019).

[27] M. Gibertini, M. Koperski, A. F. Morpurgo, and K. S. Novoselov, Magnetic 2D materials and heterostructures, Nat. Nanotechnol. **14**, 408 (2019).

[28] Z. Sun, Y. Yi, T. Song, G. Clark, B. Huang, Y. Shan, S. Wu, D. Huang, C. Gao, Z. Chen, M. McGuire, T. Cao, D. Xiao, W.-T. Liu, W. Yao, X. Xu, and S. Wu, Giant nonreciprocal second-harmonic generation from antiferromagnetic bilayer CrI_3, Nature (London) **572**, 497 (2019).

[29] H. Chu, C. J. Roh, J. O. Island, C. Li, S. Lee, J. Chen, J.-G. Park, A. F. Young, J. S. Lee, and D. Hsieh, Linear Magnetoelectric Phase in Ultrathin $MnPS_3$ Probed by Optical Second Harmonic Generation, Phys. Rev. Lett. **124**, 027601 (2020).

[30] A. McCreary, J. R. Simpson, T. T. Mai, R. D. McMichael, J. E. Douglas, N. Butch, C. Dennis, R. V. Aguilar, and A. R. Hight Walker, Quasi-two-dimensional magnon identification in antiferromagnetic $FePS_3$ via magneto-Raman spectroscopy, Phys. Rev. B **101**, 064416 (2020).

[31] T. T. Mai, K. F. Garrity, A. McCreary, J. Argo, J. R. Simpson, V. Doan-Nguyen, R. Valdes Aguilar, and A. R. Walker, Magnon-phonon hybridization in quasi-2D antiferromagnet $MnPSe_3$, arXiv:2011.12557.

[32] M. Fiebig, D. Fröhlich, B. B. Krichevtsov, and R. V. Pisarev, Second Harmonic Generation and Magnetic-Dipole-Electric-Dipole Interference in Antiferromagnetic Cr_2O_3, Phys. Rev. Lett. **73**, 2127 (1994).

[33] M. Fiebig, V. V. Pavlov, and R. V. Pisarev, Second-harmonic generation as a tool for studying electronic and magnetic structures of crystals: Review, J. Opt. Soc. Am. B **22**, 96 (2005).

[34] V. N. Muthukumar, R. Valentí, and C. Gros, Microscopic Model of Nonreciprocal Optical Effects in Cr_2O_3, Phys. Rev. Lett. **75**, 2766 (1995).

[35] M. Scagliotti, M. Jouanne, M. Balkanski, G. Ouvrard, and G. Benedek, Raman scattering in antiferromagnetic $FePS_3$ and $FePSe_3$ crystals, Phys. Rev. B **35**, 7097 (1987).

[36] E. Ressouche, M. Loire, V. Simonet, R. Ballou, A. Stunault, and A. Wildes, Magnetoelectric $MnPS_3$ as a candidate for ferrotoroidicity, Phys. Rev. B **82**, 100408(R) (2010).

[37] H. M. Rønnow, A. R. Wildes, and S. T. Bramwell, Magnetic correlations in the 2D $S = 52$ honeycomb antiferromagnet $MnPS_3$, Physica (Amsterdam) **276B–278B**, 676 (2000).

[38] A. R. Wildes, H. M. Rønnow, B. Roessli, M. J. Harris, and K. W. Godfrey, Static and dynamic critical properties of the quasi-two-dimensional antiferromagnet $MnPS_3$, Phys. Rev. B **74**, 094422 (2006).

[39] K. Okuda, K. Kurosawa, S. Saito, M. Honda, Z. Yu, and M. Date, Magnetic properties of layered compound $MnPS_3$, J. Phys. Soc. Jpn. **55**, 4456 (1986).

[40] C. Pich and F. Schwabl, Spin-wave dynamics of two-dimensional isotropic dipolar honeycomb antiferromagnets, J. Magn. Magn. Mater. **148**, 30 (1995).

[41] L. Wu, S. Patankar, T. Morimoto, N. L. Nair, E. Thewalt, A. Little, J. G. Analytis, J. E. Moore, and J. Orenstein, Giant anisotropic nonlinear optical response in transition metal monopnictide Weyl semimetals, Nat. Phys. **13**, 350 (2017).

[42] See Supplemental Material at http://link.aps.org/supplemental/10.1103/PhysRevLett.127.187201 for more experimental data and derivations, which includes Ref. [43–47].

[43] S. Lee, K.-Y. Choi, S. Lee, B. H. Park, and J.-G. Park, Tunneling transport of mono- and few-layers magnetic van der Waals $MnPS_3$, APL Mater. **4**, 086108 (2016).

[44] L. Mennel, M. Furchi, S. Wachter, M. Paur, D. Polyushkin, and T. Mueller, Optical imaging of strain in two-dimensional crystals, Nat. Commun. **9**, 516 (2018).

[45] L. Mennel, M. Paur, and T. Mueller, Second harmonic generation in strained transition metal dichalcogenide monolayers: MoS_2, $MoSe_2$, WS_2, and WSe_2, APL Photonics **4**, 034404 (2019).

[46] Z. Liu, M. Amani, S. Najmaei, Q. Xu, X. Zou, W. Zhou, T. Yu, C. Qiu, A. Glen Birdwell, F. J. Crowne, R. Vajtai,

B. I. Yakobson, Z. Xia, M. Dubey, P. M. Ajayan, and J. Lou, Strain and structure heterogeneity in MoS_2 atomic layers grown by chemical vapour deposition, Nat. Commun. **5**, 5246 (2014).

[47] Q. Zhang, Z. Chang, G. Xu, Z. Wang, Y. Zhang, Z.-Q. Xu, S. Chen, Q. Bao, J. Z. Liu, Y.-W. Mai, W. Duan, M. S. Fuhrer, and C. Zheng, Strain relaxation of monolayer WS_2 on plastic substrate, Adv. Funct. Mater. **26**, 8707 (2016).

[48] A. Ron, E. Zoghlin, L. Balents, S. D. Wilson, and D. Hsieh, Dimensional crossover in a layered ferromagnet detected by spin correlation driven distortions, Nat. Commun. **10**, 1654 (2019).

[49] M. Zhao, Z. Ye, R. Suzuki, Y. Ye, H. Zhu, J. Xiao, Y. Wang, Y. Iwasa, and X. Zhang, Atomically phase-matched second-harmonic generation in a 2D crystal, Light Sci. Appl. **5**, e16131 (2016).

[50] S. N. Neal, H.-S. Kim, K. A. Smith, A. V. Haglund, D. G. Mandrus, H. A. Bechtel, G. L. Carr, K. Haule, D. Vanderbilt, and J. L. Musfeldt, Near-field infrared spectroscopy of monolayer $MnPS_3$, Phys. Rev. B **100**, 075428 (2019).

[51] S. N. Neal, H.-S. Kim, K. R. O'Neal, A. V. Haglund, K. A. Smith, D. G. Mandrus, H. A. Bechtel, G. L. Carr, K. Haule, D. Vanderbilt, and J. L. Musfeldt, Symmetry crossover in layered MPS_3 complexes (M = Mn, Fe, Ni) via near-field infrared spectroscopy, Phys. Rev. B **102**, 085408 (2020).